

Investigations of modular microfluidic geometries for passive manipulations on droplets

D. ZAREMBA¹, S. BLONSKI¹, M. JACHIMEK¹, M.J. MARIJNISSEN¹,
S. JAKIELA², and P.M. KORCZYK^{1*}

¹Institute of Fundamental Technological Research, Polish Academy of Sciences, Pawińskiego 5B St., 02-106 Warsaw, Poland

²Department of Biophysics, Warsaw University of Life Sciences, 159 Nowoursynowska St., Building 34, 02-776 Warsaw, Poland

Abstract. Multiple pipetting is a standard laboratory procedure resulting in the compartmentalisation of a liquid sample. Microfluidics offers techniques which can replace this process by the use of tiny droplets. Passive manipulation on droplets is an interesting and promising approach for the design of microfluidic devices which on one hand are easy-to-use and on the other, execute complex laboratory procedures. We present a comprehensive study of the geometry of microfluidic components which encode different operations on droplets into the structure of the device. The understanding of hydrodynamic interactions between the continuous flow and a droplet travelling through confined space of nontrivial microfluidic geometries is crucial for a rational and efficient design of new generation of modular microfluidic processors with embedded instructions.

Key words: microfluidics, two-phase flows, droplets.

1. Introduction

Modern analytical methods (like e.g. digital PCR) often require execution of complex algorithms on numerous compartments of a sample [1]. In this context, the microfluidic technology is highly desirable, as it offers precise handling of small amounts of liquids, allows for parallelisation, integration and automation of multiple processes in a single device [2, 3]. In particular, the use of immiscible liquids allows for generation [4] and manipulation [5] on small droplets. Droplets in microfluidic channels may be considered as isolated biochemical reactors, where each single droplet has a specific composition of reagents or biological content [6, 7]. That provides incredible opportunities for performing a large number of chemical reactions or biological experiments at the same time with very small consumption of reagents and samples [8, 9].

The ability to manipulate droplets in microfluidic devices is crucial for precise control over the composition of such micro-reactors. The current state of microfluidic technology enables to perform such operations as: droplet generation, merging, splitting, moving, positioning by the use of active controllers e.g. electromagnetic valves [9–14].

The potential of the active techniques in automation of droplet traffic control is impressive [9]. However, they require the use of multiple connections and active components such as precise valves and electronics. That increases technical complexity and the cost of the whole setup, which inhibits the application of those solutions in simple in use and inexpensive

Point of Care devices. Hence the development of such systems with a wide range of liquid handling protocols remains one of the important motivations of microfluidics. Some interesting solutions exist, e.g. paper-based microfluidics [15], slip chips [16], or geometric modules for desired operations on microdroplets [17–21]. However, the simplicity of the usage is always achieved by sacrificing accuracy, the throughput and internal complexity. In order to overcome these obstacles, the next generation of lab-on-a-chip devices may contain embedded controls on the chip instead of electronics [22, 23].

In the previous publication, Korczyk et al. [24] showed examples of passive microfluidic modules called microfluidic traps. These traps were built based on two kinds of basic geometries: obstacles and slit-bypasses. Modifications of these elements and their different combinations allowed to construct traps with such functions as i) metering prescribed volume of a droplet; ii) immobilization of a droplet; iii) combining consecutive drops. The other publication by van Steijn et al. [25] demonstrated the use of slit bypasses in a construction of so-called block-and-break droplet generator. These publications presented the potential of the new approach to the construction of functional microfluidic modules. However, there is a lack of comprehensive analysis of principal mechanisms. So far rather only intuitive remarks about the operation of selected modules have been discussed. Our recent observations showed that the behaviour of droplets in some microfluidic geometries may be counter-intuitive. Hence, the intuitive approach to the design of passive elements may cost numerous failed trials and resources. Therefore, effective applications of this technology require detailed investigations on mechanisms ruling movement of droplets in nontrivial geometries [26].

The crucial role in the understanding of those mechanisms plays the confinement of flows of two liquid phases and the

*e-mail: piotr.korczyk@ippt.pan.pl

Manuscript submitted 2017-10-20, revised 2017-12-21, initially accepted for publication 2018-01-14, published in April 2018.

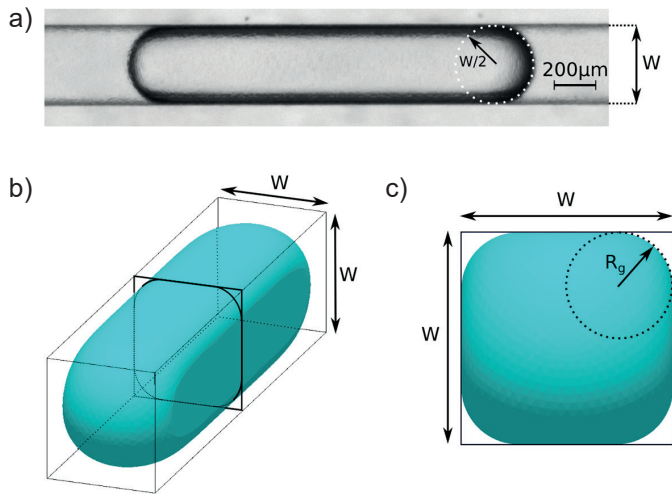


Fig. 1. The shape of a droplet confined in the channel of a rectangular cross-section: a) a micrograph of the real droplet in the channel of the width $385 \mu\text{m}$, b) and c) the simulation of the shape of a droplet in the square cross-section channel made by the use of Surface Evolver [27]. The empty corners (gutters) are visible with the radius of curvature of the interface $R_g = W/4$

confinement of the interface between them. This is the fascinating aspect of two phase flows in microfluidic channels. Microfluidics offers the unique situation when the height of the channel is lower than the capillary length, making gravity negligible. Droplets larger than the cross-section of the channel are squeezed between walls of the channel and form elongated plugs. If the vertical dimension of that cross-section is lower than the capillary length, the shape of a confined droplet is determined only by geometrical constrictions of the solid walls and by the Laplace-Young equation which describes the difference in the pressure sustained across the curved interface between two immiscible liquid phases:

$$\Delta p_L = \gamma \left(\frac{1}{R_1} + \frac{1}{R_2} \right) \quad (1)$$

where γ is the coefficient of surface tension and R_1 and R_2 are principal radii of curvature. In a static droplet both pressures, inside and outside of a droplet are constant and homogeneous. Thus the Laplace pressure drop is constant over the whole interface.

In this paper we consider droplets, which do not wet the walls of the channel (contact angle equals 180°). This condition is commonly obtained by the use of surface modifications and additions of surfactants. For the simplicity of calculations we can assume that the tips of the non-wetting droplet form hemispherical caps of both principal radii equal $W/2$. Hence the Laplace pressure drop at the tips is given by: $\Delta p_{LT} = \gamma(2/W + 2/W)$ (see Fig. 1a). Further, we assume that in the internal part of a droplet, between its cups, radius of the curvature of the interface in the direction along the axis of the channel goes to infinity. Thus, the Laplace pressure in the internal part can be described as: $\Delta p_{LI} = \gamma/R_g$, where R_g is a radius of curvature for the cross-section of a droplet in the internal part. Equating above

formulas for $\Delta p_{LT} = \Delta p_{LI}$, one can obtain $R_g = W/4$. This implies that a droplet in the channel leaves the corners filled by the continuous phase. These corners, so-called gutters, form channels parallel to the droplet, through which the continuous phase can flow around a droplet [28]. This approximated shape of a droplet is confirmed by the observations and numerical simulations of a droplet squeezed in a square-shaped channel (see Fig. 1). It is worth noticing that the equilibrium shape depends only on the dimensions of the channel and is not affected by the value of γ .

In the presence of a constant flow of continuous phase in a regular channel a plug-like droplet moves with constant speed [13, 28]. In the previous paper [24], we showed that some additional geometrical components modifying the geometry of a channel can be effectively used to disturb this movement in a controlled manner.

Let us consider two kinds of geometrical components: a bypass slit and an obstacle, which put together forms the so-called metering trap. A bypass slit is a niche of the height equal to $R_g = W/4$ placed at the top of the main channel (see Fig. 2)

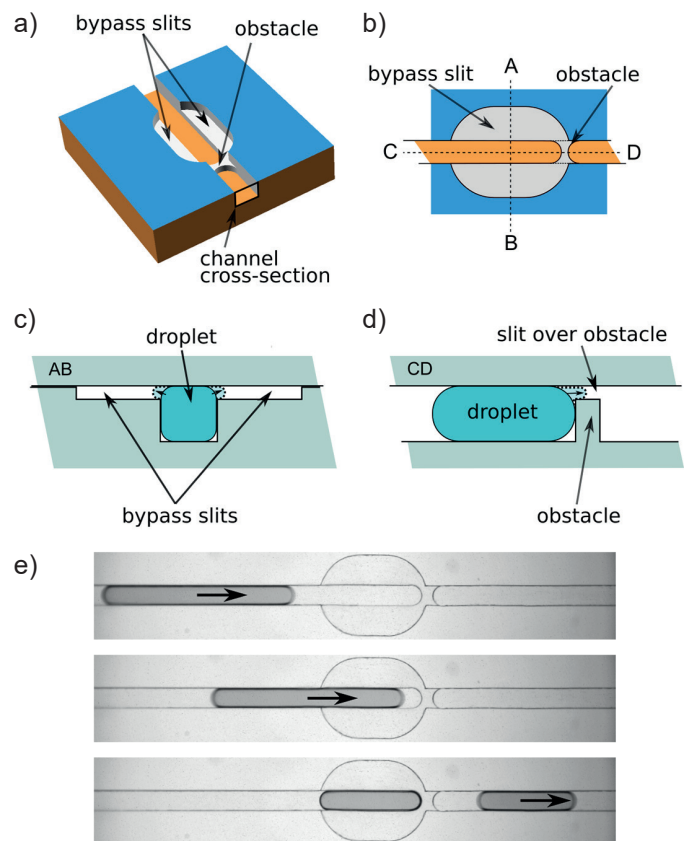


Fig. 2. The metering trap: a) 3-D visualisation of the trap with the construction elements like slit bypasses and an obstacle highlighted, b) top-view of the trap, c) and d) cross-sections through planes AB and CD as described in b). The schematic shapes of droplets in the cross-sectional picture show that the droplet needs to generate finger of the curvature much higher than the mean curvature of the static droplet to penetrate the slits of bypasses or to pass through the obstacle. e) Consecutive snapshots illustrating the main functionality of the trap. The long droplet enters a trap and is divided into two parts. One of them is immobilised in the trap, while the other one goes further

which increases the area of the cross-section of the channel. The height of the bypass equal to the radius of curvature for the interface in gutters, ensures that the shape of a static droplet is not affected by the presence of this slit. Indeed, the bypass slit is an additional narrow channel, which enlarges the gutter. Similarly, like in the regular square channel, the corners cannot be occupied by the static droplet. The role of these additional slits is to enhance the bypass flow of continuous phase.

The other geometrical element we used for the construction of our traps is an obstacle in the main channel, which locally decreases the lumen of the channel. To go across the obstacle, a droplet needs to create a tip with a higher curvature than the curvature in the rest of the channel. This means that additional pressure must be applied to let the droplet pass the barrier. As we have shown before, the combinations of traps allowed for encoding of a digital sequence of operations on droplets. This allowed for a controlled exchange of mass between droplets generating desired distributions of compound concentrations [24]. Despite the previous publication describing traps and whole complex systems of traps, there is still a lack of knowledge about their principal mechanisms. At this point, there are only some, rather intuitive remarks about the operation of traps, which allowed to design a few types of traps through trial and error. The further development of this very promising method requires detailed fundamental investigations.

Here we propose a comprehensive approach that gives insight into mechanisms which are responsible for the specific features of traps. We conducted our analysis on the example of the metering trap. We present the results of both experimental and numerical investigations and show the complex interactions between the droplet and the flow of the continuous phase altered by the confined geometry of the metering trap. The gathered knowledge is vital for the understanding of the principle of passive structures.

2. Materials and methods

The microfluidic devices were fabricated of a transparent polycarbonate plate (Bayer, Makrolon® GP, Germany) of 5 mm thickness via direct milling using a CNC milling-engraving machine (Ergwind, MFG4025P, Poland). During the milling process a polycarbonate plate was fastened to the perforated vacuum table of the CNC machine by applying underpressure (0.4 bar), generated by a vacuum pump (AGA Labor, Basic 20, Poland), which ensured the high precision of mounting of milled material in the Z axis. A 2-flute fishtail milling bit FR208 of diameter 385 μm was used for engraving the channels. For the optimization of the fabrication process, the diameter of the milling tool was set to the width of the main channel W . The half of that diameter sets the minimal radius of the curvature which can be engraved in the plane of the device. In consequence of that geometrical constraint, both faces of the obstacle must be round (with radius equal $W/2$) and concave (see Fig. 2). This shape is compatible with the round and convex shape of the tip of a droplet, which is as well determined by the width of the channel. Engraved structures were cleaned out with

a high-pressure water washer (Karcher, K7 Premium, Germany) and further washed by hand with isopropanol. In the next step, channels were closed by bonding the milled chip with another polycarbonate plate with the use of a heating press (Argenta, AW03, Poland) at a temperature of 135°C and a pressure of 0.1 bar cm^{-2} . The chip was kept in the press at high temperature for about 30 minutes, then allowed to cool down all the time under pressure. Before the bonding procedure the holes of diameter 800 μm were drilled through one of the plates to form inlets and outlet to the channels of the milled device. Pieces of cut needles of the outer diameter 800 μm (Braun, Sterican, Germany) were fixed into the inlet and outlet holes and used to enable tight connection with elastic tubing.

The n-Hexadecane 95% (Alfa Aesar, Germany) was used as the continuous phase (CP) and distilled water coloured with ink (Pelikan 4001, Germany) was used as a droplet phase (DP). The surfactant (Span-80, Fluke Analytical, Germany) was added to the n-Hexadecane with concentration of about 0.2% to avoid the wetting of the walls of channels by the droplets. The n-Hexadecane density is 0.773 gml^{-1} and dynamic viscosity is 3.0041 mPas at 25°C. Interfacial tension between n-Hexadecane and water is 0.0048 $\text{Nm}^{-1} \pm 0.0002$ measured by the pendant drop method.

Experiments consisted mainly of visual observations of flows in fabricated transparent microfluidic devices. Liquids were pumped by precise and pulsation-free syringe pumps (neMESYS, Cetoni GmbH) equipped with 1.0 ml syringes made of borosilicate glass with a PTFE plunger (ILS Innovative Labor Systeme GmbH). Syringes were connected with the microfluidic device using polyethylene tubing with inner and outer diameter equal to 0.76 mm and 1.22 mm, respectively (Intramedic®, Becton Dickinson Co.). Droplets are created with the use of a T-junction geometry. The flow rate of the CP was 0.75 mlh^{-1} both for droplet creation and its displacement.

Flows investigated in the microfluidic device were visualised using a Huvitz HSZ-645TR stereoscope equipped with 0.5 \times objective and IDS UI-3274-LE-C-HQ digital camera. Recorded images were stored on a PC computer for further analysis.

Velocity field of the flow of the CP through the trap was determined using particle image velocimetry technique (PIV) [29, 30]. The analysed flow was seeded by glass spheres (tracer particles) with a diameter of 12 μm and density similar to the liquids, to minimise buoyancy effects. Images were registered using the pco.1200hs high speed digital camera (PCO Imaging) and Nikon Eclipse E-50i microscope equipped with an 10 \times /0.3 objective (Nikon LU Plan Fluor). Characteristics of the recording system provided 519.5 pixel/mm resolution of the captured images. The recording framerate was set to 100–200 fps (depending on the flow velocity) to ensure the displacement of the tracer particles in the range of 10–15 pixels between sequential frames. The appropriately short exposure time (100 μs) prevented blurring of the images of tracer particles due to their motion. The evaluation of images was performed using the commercial software VidPIV (ILA GmbH). To obtain instantaneous velocity fields, cross-correlation was applied with the interrogation window 128 \times 128 pixels and spatial window separation equal to 32 pixels in both directions, X and Y. After

this preliminary evaluation, a local median velocity filter was applied to compare each vector with a median of the nearest neighbours ($i \pm 2$) and errors were removed. Filtered out wrong vectors were replaced with vectors determined as an interpolated value of neighbours ($i \pm 2$). In the second, final step of evaluation, adaptive cross-correlation (interrogation window equal to 128×128 pixels and spatial window separation equal to 16 pixels in both directions) and a local median filter were applied. As a result we obtain more than 1000 instantaneous velocity fields for the whole process of droplet flow through the trap.

We used the Multiskan Go Microplate Spectrophotometer (Thermo Scientific) to measure the absorbance of the mixture collected in the PMMA UV cuvettes (BRAND, Germany) with a minimum filling volume of 1.5 ml. The quantity was measured directly with the use of the spectrophotometer was absorbance, which according to the Beer–Lambert law is proportional to concentration. So the ratio of flows was estimated directly as the ratio of absorbance measurements. This makes the estimation independent from possible fluctuations of starting concentration. In all presented experiments we used as an indicator sodium pyruvate (Sigma-Aldrich, Germany) in aqueous solution with starting concentration $C_0 = 100 \text{ mmol l}^{-1}$. As the buffer liquid we used distilled water.

For the numerical analysis of the motion of droplets, the volume-of-fluid (VOF) model [31] implemented in ANSYS Fluent was used to simulate the interactions between two liquid phases. This technique uses the finite volume method to solve the Navier-Stokes equations with an additional volume fraction function α , which takes 0 for one of the phases, and 1 for the other. The evolution of the interface is introduced by the transport equation:

$$\frac{\partial \alpha}{\partial t} + \nabla \cdot (\mathbf{u}\alpha) = 0, \quad (2)$$

where \mathbf{u} – fluid velocity vector. The density and viscosity of the fluid are obtained as:

$$\rho = \alpha\rho_1 + (1 - \alpha)\rho_2, \quad (3)$$

$$\mu = \alpha\mu_1 + (1 - \alpha)\mu_2. \quad (4)$$

The remaining equations are the incompressible Navier-Stokes equations:

$$\nabla \cdot \mathbf{u} = 0, \quad (5)$$

$$\frac{\partial \rho \mathbf{u}}{\partial t} + \nabla \cdot (\rho \mathbf{u} \mathbf{u}) = -\nabla p + \nabla \cdot [\mu(\nabla \mathbf{u} + \nabla \mathbf{u}^T)] + \gamma \frac{p \mathbf{k} \mathbf{n}}{\frac{1}{2}(\rho_1 + \rho_2)}, \quad (6)$$

where p – pressure and t – time. The last term in the momentum equation refers to the surface tension. In it γ , k and \mathbf{n} represent the surface tension coefficient, the curvature and the surface

normal, respectively. A variable time stepping method was used allowing the time step to be changed between 1×10^{-7} s and 1×10^{-4} s, predominantly the time step oscillated around 1.5×10^{-5} s. To ensure correct representation of the droplet shape and its movement, the computational mesh should have at least 20×20 regular elements in the cross-section of the central channel, in the plane perpendicular to the droplet movement. This leads to the entire domain, showed in Fig. 3, consisting of 275,302 finite volumes. The use of a rarer mesh would cause interface dispersion.

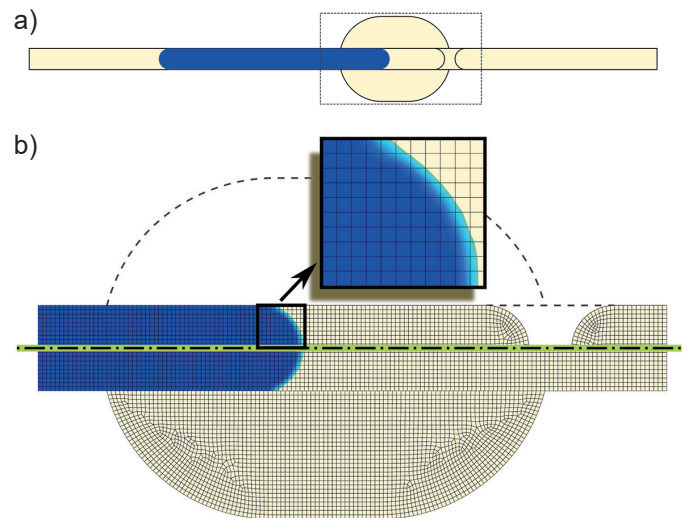


Fig. 3. The mesh used in the simulations. a) an overview of the whole domain with a droplet inside. b) close-up on the trap itself. The composition of two horizontal cross-sections of the simulation mesh taken at two different heights. The top part – at half of the height of the domain (below the bypasses, the obstacle visible), the bottom part – at half of the height of the bypasses (the obstacle invisible). The colours represent the volume fraction of the droplet (blue = droplet).

The inset – magnification of the interface of the droplet

3. Results

3.1. Experimental observations of kinetics. Herein we present the experimental analysis of two distinguished examples of flow of droplets through the metering trap. In the first one, we considered a short droplet (of the length not longer than the length of a trap L_T , see Fig. 4). In the other case, we investigated the flow of a long droplet (of the length longer than L_T , see Fig. 5). In both cases, we used the same metering trap. The flow of a droplet was driven by the flow of CP pumped into the microfluidic device with a constant flow rate $Q_C = 0.75 \text{ ml h}^{-1}$. It is worth noting that the use of syringe pumps ensured the constant flow rate regardless of fluctuations of pressure generated by the droplet travelling through the trap. Before the experiments, droplets had been formed in the T-junction by the injection of the desired volume of droplet phase followed by the switching on of the continuous phase's flow.

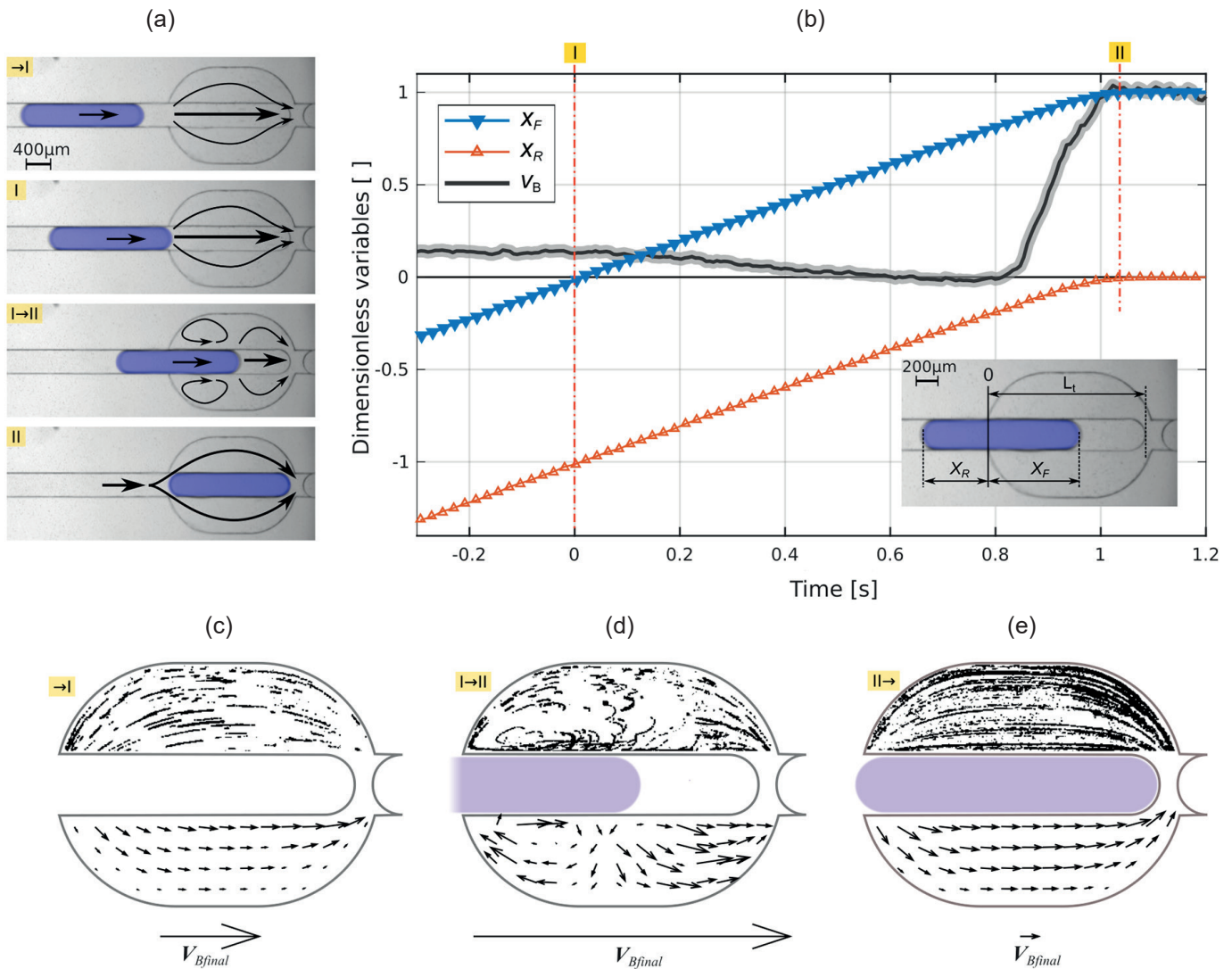


Fig. 4. The kinetics of the flow in the case of a short droplet entering the metering trap. a) Consecutive snapshots showing the moving droplet in different stages and the schematic reconstruction of the flow pattern of continuous phase. b) The measurement of the main kinetic quantities: x_F – position of the front of the droplet, x_R – position of the back of the droplet, v_B – average velocity of the CP in the bypass slit. The estimated errors of measurements of v_B displayed as the accompanying wide grey line. The errors of other quantities were of the order of widths of the displayed lines. c) – e) Experimental visualization of flow patterns in the bypasses in different stages: c) – period →I and stage I, d) period I→II, e) stage II and period II→. The top bypasses – traces of particles, the bottom bypasses – velocity fields measured by PIV. Note different scaling of vectors in the visualisation of different stages. For comparison, the same vector of the constant length V_{Bfinal} is displayed below in the scale of the corresponding velocity field

3.1.1. A short droplet case. The previous observations showed that a droplet which the length is not longer than the internal length of the trap L_T becomes immobilised in the metering trap [24]. This process is illustrated in the snapshots (Fig. 4a). We can see that first the droplet approaches the trap from the left side driven by the constant flow of the CP and finally stops in the trap regardless the fact that the flow of the CP is still the same.

For a better understanding of the spontaneous transition from the initially unsteady flow to finally steady flow, we conducted a series of observations of the kinetics. The quantitative description of the process is provided by the conducted measurements. By the use of high-speed cameras and image

processing, we measured the position of the front of a droplet X_F and the positions of its back X_R in time. Simultaneously we measured the velocity field in the bypasses with the use of the PIV technique. In the plot we present the normalised variables: $x_F = X_F/L_T$, $x_R = X_R/L_T$. The value V_B was obtained by spatial averaging of the component of the velocity field parallel to the main channel in the bypasses. Then the normalised value v_B was calculated dividing V_B by V_{Bfinal} – the time average of V_B for a stationary flow after the droplet finally stops in the trap. In this final configuration the V_B reaches its maximum value, hence the maximum level of $v_B = V_B/V_{Bfinal}$ is approximately equal to unity.

On the base of measurements the process can be disassembled into three particular periods with two critical stages between them: stage I, when the front of the droplet reaches the entrance of the trap ($x_F = 0$) and stage II, when the front of the droplet reaches the obstacle ($x_F = 1$). At stage II the front of the droplet stops at the obstacle. In this moment, due to the short length of the droplet equal (or shorter) to the length of the trap L_T , the whole droplet is inside the trap: the front of the droplet touches the obstacle ($x_F = 1$) and its back ($x_R \leq 0$) opens the entrance to the bypasses for the flow of the CP. After that, the flow of the CP around the immobilised droplet becomes stationary.

Our observations showed that before a droplet enters the trap (stage \rightarrow I) it moves with a constant speed and the observed flow in the bypasses is as well constant. Between stage I and stage II the droplet enters into the trap. The flow in the bypasses decreases. This means that the droplet efficiently blocks the inflow of the CP into the bypasses. Once the front of the droplet reaches the barrier ($x_F = 1$) the droplet stops and v_B reaches its maximum value. After stage II the flow becomes stationary, where the droplet is immobilised in the trap and the entire flow of the CP flows around the droplet through the bypasses.

These observations show the interactions between the flows of the two phases in the confined geometry of the trap. Until stage I the flow of the CP in the trap is stationary with the main flow through the central channel and a minor flow passing through the bypasses. In the period between stage I and stage II the droplet effectively switches off the CP flow through the bypasses. It is worth noting, that the flow topology of this period differs from that of other periods. The significant distinction is the presence of additional single circulation zones in each of the bypasses appearing behind the line marking the front of the droplet (see Fig. 4a and d). While the droplet continuously moves forward, the circulation zone (with zero average velocity) enlarges. The consequence of that is the gradual fall of the average velocity in the bypass v_B (see Fig. 4b). After stage II the back of the droplet stops in such a position, that opens a way for the CP into the bypasses and the flow of the CP around the droplet becomes mainly unidirectional and much larger than before stage I. This trap construction utilizes the barrier to hold the droplet in place. It is possible because the viscous pressure drop (due to the flow of the CP around the droplet) is smaller than the capillary breakthrough pressure (required to move the droplet across the barrier).

3.1.2. A long droplet case. In this case we consider the movement of a droplet of the length $2L_T$ – a double length of the trap. We analyzed the kinetics of the process, likewise as in the previous example, measuring such variables as: x_F , x_R and v_B (see the inset in Fig. 5a). Unlike as for a short droplet, in the case of the long one, we observed that the droplet temporarily expands penetrating the slits of the device (Fig. 5b). To take that into account we introduced two additional measured variables W_N and W_I . W_N is the width of the so-called neck (see the inset in Fig. 5a). The neck forms when a droplet is passing across the barrier. It is a liquid bridge connecting two parts of

the droplet on two sides of the barrier. The plotted value of the width of the neck was normalized by the width of the channel: $w_N = W_N/W$. W_I is the width of the side intrusions of a droplet penetrating into the bypasses. The value plotted in Fig. 5a was calculated by averaging the width of intrusions from both sides of a droplet and normalised by W_B – the width of the bypass: $w_I = W_I/W_B$.

On the base of observations and the evolution of measured variables we distinguished 7 critical stages of the process, that we describe below. In stage I the front of the droplet reaches the entrance to the trap ($x_F = 0$). In stage II the tip of the droplet reaches the obstacle ($x_F = 1$). Within the period (I–II) the droplet blocks the flow of the continuous phase to the bypasses, what can be observed in the measurements of v_B . Until stage II the case of the long droplet is similar to the case of the shorter droplet. Just after stage II the front of the droplet is held by the obstacle ($x_F = const = 1$), while the back (in the inlet channel) is still effectively pushed by the flow of the CP. The squeezed droplet is forced to penetrate the bypasses, which is marked by the rise of w_I . In stage III we observe the critical point, where the continuously pushed droplet starts to penetrate the slit over the obstacle (rise of x_F). During the period III \rightarrow IV, the front of a droplet ($x_F > 1$) starts to move passing across the obstacle and developing the neck ($w_N > 0$). In stage IV both the width of the neck w_N and the intrusions to the bypasses w_I reach their maximum values. The front of the droplet has passed the obstacle and starts to move with a constant speed in the outlet channel (linear growth of x_F).

Stage V – the back of the droplet reaches the entrance to the trap ($x_R = 0$) and allows the CP access to the bypasses. The force pushing the back of the droplet drops rapidly and the back of the droplet stops ($x_R = const = 0$). After stage V the intrusions of the droplet in the bypasses (w_I) recede and are being replaced by an incoming flow of the CP. This generates the flow of the DP through the obstacle inflating the part of the droplet at the front. In stage VI the droplet neck starts shrinking (w_N decreases) and finally breaks in stage VII ($w_N = 0$). This results in the division of the droplet into two separate parts. One of them is kept immobilised in the trap and the rest of the droplet continues the movement with a constant speed.

These observations of kinetics show that the confined flow of both phases directly depends on the current position of both the front x_F and the back x_R of a droplet. The different stages with the different morphology of flow fields are triggered respectively to the position of a droplet relative to the geometry of a trap. Hence the length of a droplet and the geometry of a trap are crucial for the functionality of a trap and their behaviour can be tailored by the proper use of different elements.

Better insight into the dynamics of this process can be provided by numerical simulations, as presented in the next subsection.

3.2. Volume of fluid simulation. We performed numerical simulations of the partitioning process of the long droplet (double of the length of a trap L_T) in the metering trap. The simulation domain consisted of a complete 3D geometry of the trap identical to the design used in the experiments. The input and

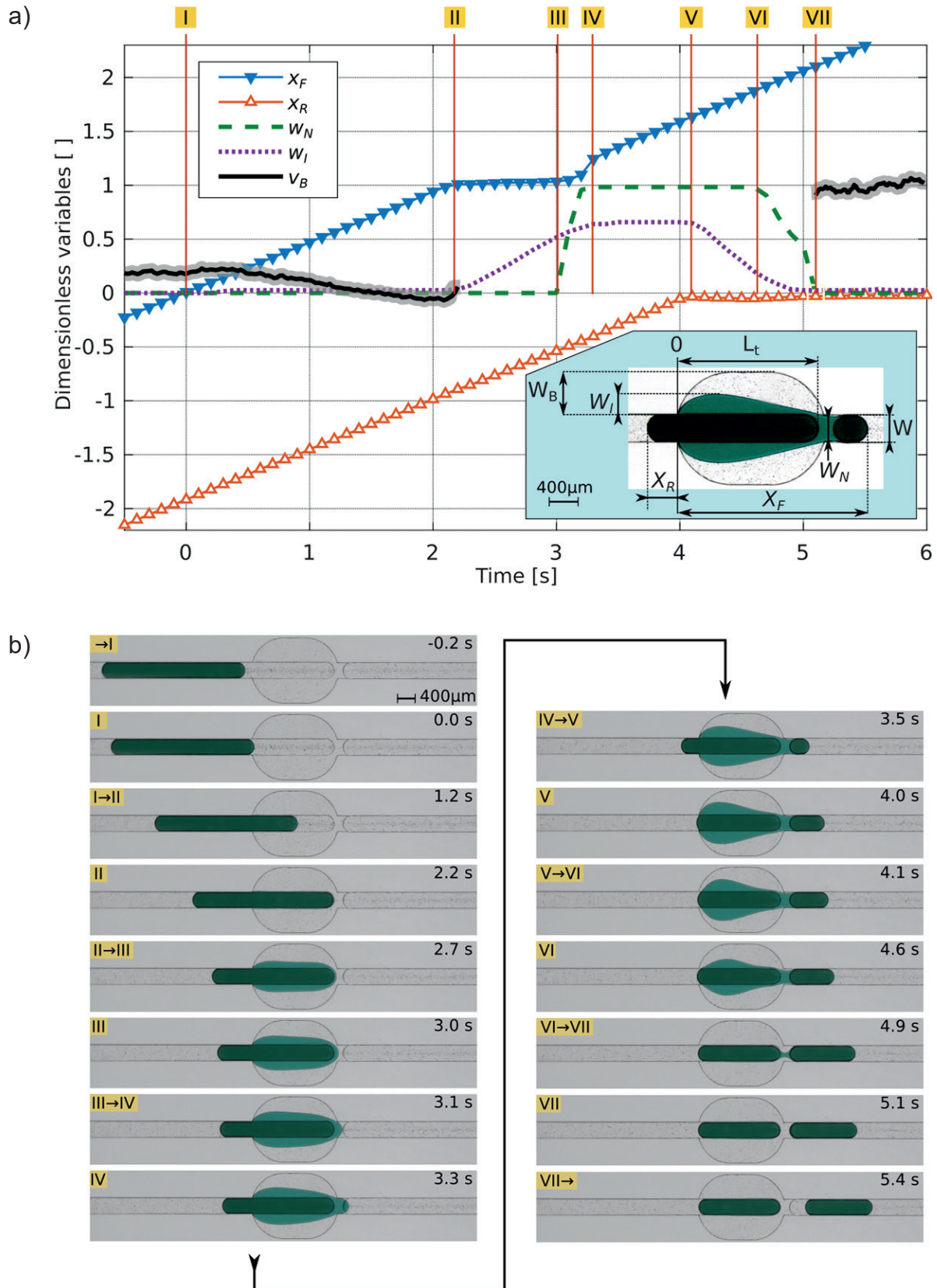


Fig. 5. The analysis of the kinetics in the case of the passage of a long droplet through the metering trap: a) the time plot of measured kinetic characteristics as shown in the inset; v_B – average velocity of the CP in the bypass slit. The estimated errors of measurements of v_B displayed as the accompanying wide grey line. The errors of other quantities were of the order of widths of displayed lines. b) consecutive snapshots recorded during experimental observation

output channels in the simulations, on the one hand, they were shortened to minimize the size of the domain and optimize the computation time, on the other hand, were sufficiently long to enable the observation of the whole investigated process with all the critical stages. The simulation domain is shown in snapshots in Fig. 6b. The constant rate of flow of the CP was fixed at the inlet of the device, what simulate the use of syringe pumps in experiments.

The numerical simulations reveal the same main feature of the metering trap as observed in the experiments. A droplet is partitioned into two parts, where one of them is immobilized in the trap. The comparison of snapshots from simulation and experiments reveals some quantitative differences visible in shapes of the bypass intrusions in stages from III to V (compare snapshots in Fig. 5b and Fig. 6b). They were caused by the imperfections introduced during the fabrication process of the real device. During the bonding, the high temperature and pressure caused the slight collapse of bypasses in the central region of the trap. So the extent of intrusion of the real droplet in the central part of bypasses is lower than in the case of the simulation. Regardless those discrepancies between experiment and simulations, we can distinguish in both situations the same stages of the process. What is more important by the mean of simulations we can analyze the evolution of the pressure in the inlet of the computational domain. In the system driven by a constant flow-rate, the pressure may evolve due to the changes of the hydraulic resistance of the flow. Fig. 6a presents the evolution of the pressure difference Δp between the inlet and the outlet of the device.

The pressure starts to grow very fast after stage II. We can see in Fig. 6a that the period II \rightarrow III can be divided into two distinct parts with different pressure rise rates. We interpret

the first part as the fast build-up of the breakthrough pressure required for the penetration of the slit. In order, to penetrate the narrow slit a droplet needs to develop the interface with the radius of curvature equal to half of the height of the slit (see the inset with the cross-section of the trap in Fig. 6a). In the second part, during the expansion of the droplet into the bypasses the curvature of the interface grows only in the horizontal plane (curvature and its changes are much lower than in the vertical plane), which results in a much lower slope, which is illustrated in the corresponding inset in Fig. 6a.

Between stage III and stage IV, the pressure grows fast and reaches its maximum value. That jump of pressure corresponds to the breakthrough pressure for the obstacle. In the period III \rightarrow IV the droplet develops the neck and then, in the period V \rightarrow VI, grows behind the barrier. Once the neck breaks in stage VII the pressure grows again reaching the terminal level. The terminal pressure is higher than before the entrance of the droplet into the trap. This fact can be explained by the change of the geometry of the flow of the CP through the trap. The trapped droplet occupies the central part of the trap forcing the CP to flow entirely through the bypasses. The hydraulic resistance of such restricted flow of the CP is higher than the resistance of the empty trap. It is very interesting and worth noticing that the pressure after the break-up of a droplet is even higher than the pressure during the process of the pumping of a droplet through the obstacle (V \rightarrow VI).

To understand this fact we should consider the whole process again. During the periods II \rightarrow IV the pressure is increased and the part of the work exerted on the deformation of a droplet is accumulated in the potential energy of shape deformation. From stage IV to VI this energy is recovered during the process of receding of the droplet from the slits of the bypasses.

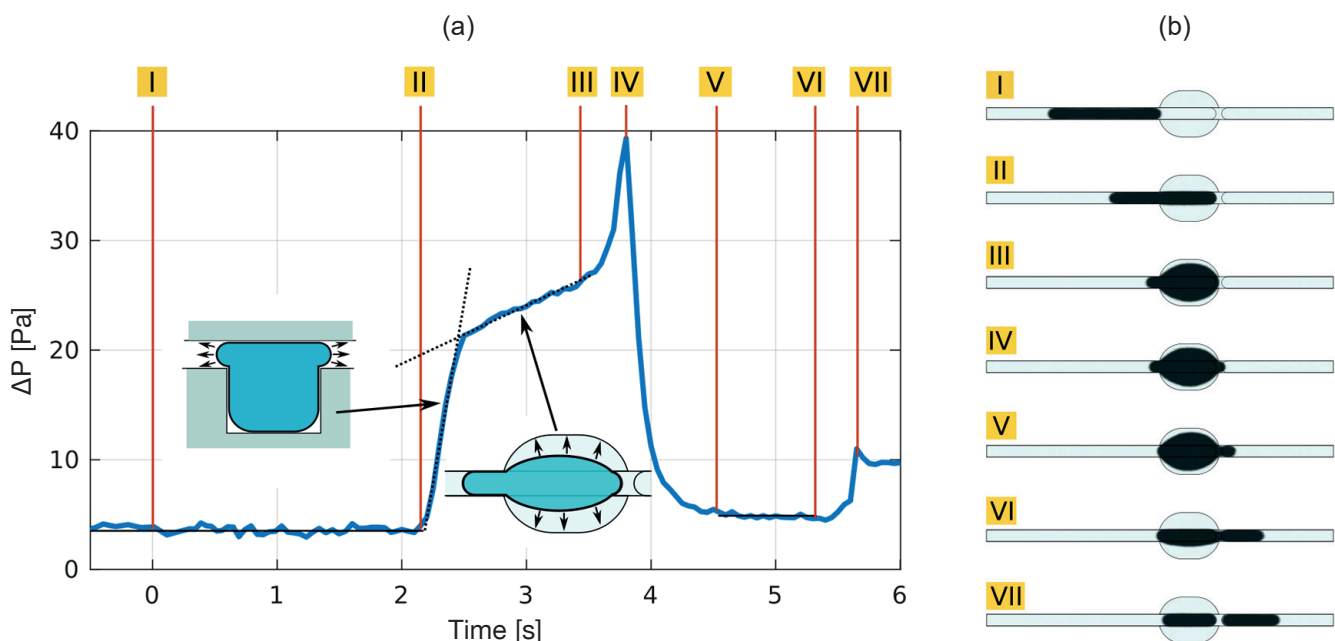


Fig. 6. Results of numerical simulations of the process of a droplet passage through the metering trap: a) time plot of pressure difference Δp along the device, b) top view of the simulation domain with a contour of the droplet in distinguished stages

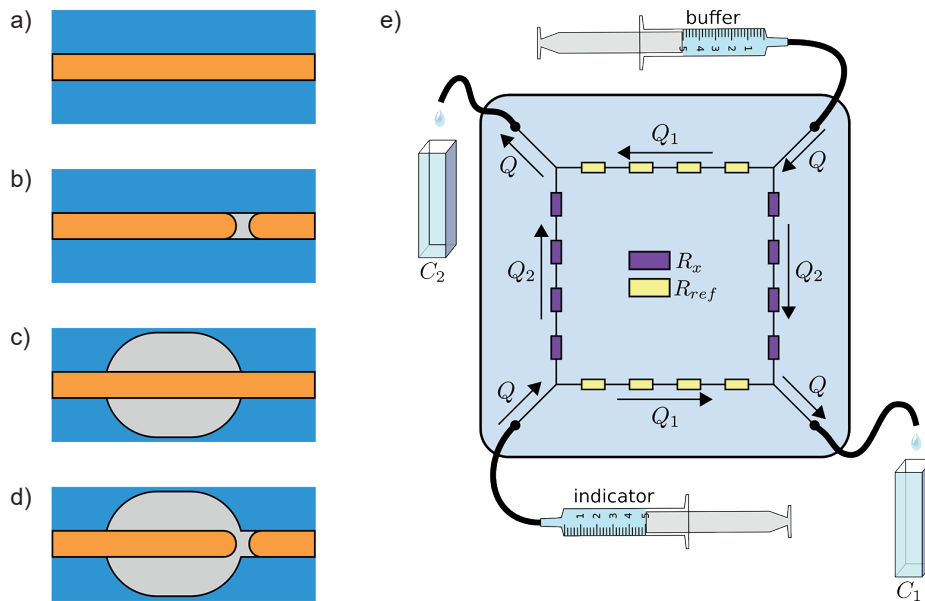


Fig. 7. The measurement method of hydraulic resistance: a) the reference channel, b) the channel only with obstacle, c) the channel only with bypass, d) the channel with full metering trap, e) the device used to measurement of hydraulic resistance

3.3. Measurements of the hydraulic resistance. As we showed in the previous paper [24], the most promising perspective for the application of traps is to use multiple of them in specially designed combinations. Such modular architectures can create integrated circuits with embedded algorithms. The design procedure of such complex microfluidic networks usually utilizes the so-called electric circuit analogy [32]. In this approach, the distribution of flow between junctions of the microfluidic network is predicted by the use of the equivalent electric circuits where each part of the network is characterized by a constant parameter – the hydraulic resistance R .

That resistance describes the relationship between the flow-rate Q and the pressure difference along the fluidic element:

$$R = \Delta p / Q. \quad (7)$$

For a Hagen-Poiseuille flow through a regular channel the resistance is a function of the dynamic viscosity μ , the length of the channel L and its cross-sectional area A :

$$R = \frac{\alpha \mu L}{A^2} \quad (8)$$

where α is a dimensionless geometrical correction factor, which depends on the shape of the cross-section of the channel [33].

The resistance of irregular elements such as the microfluidic traps can be estimated via the numerical simulations [34] or measurements [35, 36]. The numerical simulations seem to be a most convenient tool, however, it is often very difficult to include all imperfections of the fabrication procedure as well as the material properties [34]. Hence the measurements of the hydraulic resistance of irregular elements are of high importance. According to the equation, it can be done by the measurement of

the pressure difference Δp . However, the integration of pressure sensors with the device is technically challenging [35] and the accuracy of this method is limited by a relatively low pressure drop generated by microfluidic elements and the sensitivity of sensors. The alternative method presented by Choi et al. [36] consists of microscopic observations of the interface between parallel flows in a specially designed device.

In this paper, we present our original approach towards the estimation of the resistance. The advantage of the proposed method is the use of the spectrophotometric measurements of the concentration of the indicator dye in a microfluidic device consisting of the investigated resistance and the reference resistance. The main part of the resistance comparator constitutes of a rectangle with replicated resistive elements (Fig. 7e). Each side of the rectangle consists of a number of reproduced and serially connected elements of the same geometry. The opposite sides of the rectangle are identical. One pair of the opposite sides consists of the replicated geometry of unknown resistance R_x , while the other pair consists of the replicated reference geometry of resistance R_{ref} . The reference geometry was just the regular rectangular channel (see Fig. 7a). We investigated the resistances of three different geometries: i) a channel with an obstacle (Fig. 7b), ii) a channel with bypasses (Fig. 7c), and iii) the complete metering trap (Fig. 7d). The first two geometries were the components of the metering trap so that we could analyze resistances of them separately. As showed in Fig. 7a–d each single fluidic module consisted of the channel of the length equal to ten widths of the channel W . Such modules were replicated in the test device.

Two inlets to each device were placed in the opposite corners of the rectangle. Importantly, one of the inputs was fed with the clear buffer, while the other one with the solution of the buffer and the indicator. Two outputs of the device were placed

in the other pair of diagonal corners. Thus the device possesses the symmetry concerning the rotation by an angle of 180° .

In order to obtain the same symmetry of flows, we took care to ensure the uniform conditions at both inlets, as well as uniform conditions at both outlets. If all these conditions are satisfied the input streams of equal flow rates Q are divided at the input junctions in the same proportions, each of them into two flows Q_1 and Q_2 . Then they meet at the outputs so that the flow Q_2 of the buffer mixes with the flow of the indicator Q_1 in the right bottom corner (relative to the Fig. 7c). In the opposite corner, the flow of buffer Q_1 mixes with the flow of indicator Q_2 . The output concentration of the indicator in both outputs C_1 and C_2 are simply given by ratios of flows:

$$C_1 = C_0 \frac{Q_1}{Q}, \quad (9)$$

$$C_2 = C_0 \frac{Q_2}{Q}, \quad (10)$$

where C_0 is the initial concentration of the indicator introduced into the inlet of the device. The equation 7 implies:

$$n_1 R_{ref} = \Delta p_1 / Q_1, \quad (11)$$

$$n_2 R_x = \Delta p_2 / Q_2, \quad (12)$$

where n_1 and n_2 are the numbers of replicated resistive elements. Δp_1 and Δp_2 are the pressure drops along two types of sides of the internal rectangle of the device. Due to the symmetry of flows, pressures at both inlet corners are equal as well as pressures at both output corners are equal, so: $\Delta p_1 = \Delta p_2$. If $n_1 = n_2$ (in our case $n_1 = n_2 = 4$), solving equations 9–12 we obtain the ratio of resistances given by the following equation:

$$\frac{R_x}{R_{ref}} = \frac{Q_1}{Q_2} = \frac{C_1}{C_2}. \quad (13)$$

Equation 13 implies that the measurements of relative resistance requires only measurements of concentrations of the indicator C_1 , and C_2 . Due to that fact, the experimental procedure for estimation of the resistance is relatively simple. During the measurements both liquids were pumped with the same flow rates $Q = 5 \text{ ml h}^{-1}$ by the use of syringe pumps. After flushing the channels for 3–5 min and eliminating the bubbles to stabilize the flow, 1.5 ml of the solutions were collected in two UV spectrophotometric cuvettes via tubing of equal lengths. The collecting cuvettes were placed at the same level, which ensured equal pressure at both outlets. In order to reduce evaporation and changes in the concentration of the liquids the cuvettes were closed at the end of every experiments. After that the measurements of concentration from each cuvette were performed by the use of a spectrophotometer. Measurements were repeated at least 3 times and the averaged results with standard deviation calculated for each series are presented in Table 1.

Table 1

Measurements of the relative resistance R_x/R_{ref} for selected microfluidic geometries: the obstacle, the bypass and the metering trap (see Fig. 7b–d)

	obstacle only (b)	bypass only (c)	metering trap (d)
R_x/R_{ref}	2.15	0.939	2.17
standard deviation	0.02	0.003	0.01

The results showed the intriguing fact that the addition of slit-bypasses to the channel does not change significantly the resistance despite of the increase of the cross-section. In the case of the obstacle, on the contrary, even short obstacle, introduces a significant rise of resistance. The advantage of the above proposed method is the simplicity of the whole procedure. As the spectrophotometer is a very common instrumentation, hence this method can be widely available for the researchers working on microfluidics.

We performed additional numerical simulations for the metering trap obtaining a value of 1.74 for the relative resistance of the metering trap. It is significantly lower than the value of 2.17 obtained in the experiments. This discrepancy can be explained by the discussed before deformation of a real device caused mainly by the bonding procedure. The fabricated device is slightly collapsed, what we observed during the investigation of the motion of droplets. In the result the resistance of the fabricated device is higher than the design. This shows that although the numerical simulations are very valuable for the investigations of the principal mechanisms, the more reliable characteristics of real systems can be achieved in the course of experiments.

4. Conclusions

In this paper, we presented the comprehensive analysis of the movement of a droplet through the complex microfluidic geometry – the metering trap. We utilised a set of such tools as image processing based measurements of kinetic properties, PIV measurements of velocity fields, the Volume Of Fluid simulations and measurements of hydraulic resistance. Those tools, coupled together, provide the detailed description of the interactions between two immiscible liquid phases altered by the geometry of the trap. The above analysis was conducted on the example of the metering trap, however, it can be adapted to other geometries. The detailed analysis shows the rich complexity of the flow of a droplet confined by solid walls. As we expected, during the flow of that droplet through traps structures the bypasses are activated or deactivated depending on the actual position of a droplet. That mechanism can be used in triggering specific operation on droplets as merging, splitting or trapping. Combinations of such operations enable the design of microfluidic architectures with embedded algorithms. The understanding of the mechanisms investigated in this paper is crucial for the optimisation of hydrodynamic traps and effective design of new modules with additional desired features.

Acknowledgements. Project operated within the grant 2014/14/E/ST8/00578 financed by National Science Centre, Poland. S.J. acknowledges financial support from the Polish National Science Centre under the grant Opus 8 no. 2014/15/B/ST4/04955.

REFERENCES

- [1] F. Shen, B. Sun, J.E. Kreuzt, E.K. Davydova, W. Du, P.L. Reddy, L.J. Joseph, and R.F. Ismagilov, "Multiplexed Quantification of Nucleic Acids with Large Dynamic Range Using Multivolume Digital RT-PCR on a Rotational SlipChip Tested with HIV and Hepatitis C Viral Load", *Journal of the American Chemical Society* 133 (44), 17705–17712 (2011)
- [2] G.M. Whitesides, "The origins and the future of microfluidics", *Nature* 442 (7101), 368–373 (2006)
- [3] S.-Y. Teh, R. Lin, L.-H. Hung, and A.P. Lee, "Droplet microfluidics", *Lab on a Chip* 8 (2), 198 (2008)
- [4] P. Garstecki, A. Ganan-Calvo, and G. Whitesides, "Formation of bubbles and droplets in microfluidic systems", *Bull. Pol. Ac.: Tech.* 53 (4), 361–372 (2005)
- [5] A.M. Pit, M.H.G. Duits, and F. Mugele, "Droplet Manipulations in Two Phase Flow Microfluidics", *Micromachines* 6 (11), 1768–1793 (2015)
- [6] H. Song, D.L. Chen, and R.F. Ismagilov, "Reactions in Droplets in Microfluidic Channels", *Angewandte Chemie International Edition* 45 (44), 7336–7356 (2006)
- [7] A.B. Theberge, F. Courtois, Y. Schaerli, M. Fischlechner, C. Abell, F. Hollfelder, and W.T.S. Huck, "Microdroplets in Microfluidics: An Evolving Platform for Discoveries in Chemistry and Biology", *Angewandte Chemie International Edition* 49 (34), 5846–5868 (2010)
- [8] K. Churski, T.S. Kaminski, S. Jakiela, W. Kamysz, W. Baranska-Rybak, D.B. Weibel, and P. Garstecki, "Rapid screening of antibiotic toxicity in an automated microdroplet system", *Lab on a Chip* 12 (9), 1629–1637 (2012)
- [9] S. Jakiela, T.S. Kaminski, O. Cybulski, D.B. Weibel, and P. Garstecki, "Bacterial Growth and Adaptation in Microdroplet Chemostats", *Angewandte Chemie International Edition* 52 (34), 8908–8911 (2013)
- [10] S. Zeng, B. Li, X. Su, J. Qin, and B. Lin, "Microvalve-actuated precise control of individual droplets in microfluidic devices", *Lab on a Chip* 9 (10), 1340–1343 (2009)
- [11] B.-C. Lin and Y.-C. Su, "On-demand liquid-in-liquid droplet metering and fusion utilizing pneumatically actuated membrane valves", *Journal of Micromechanics and Microengineering* 18 (11), 115005 (2008)
- [12] K. Churski, P. Korczyk, and P. Garstecki, "High-throughput automated droplet microfluidic system for screening of reaction conditions", *Lab on a Chip* 10 (7), 816–818 (2010)
- [13] S. Jakiela, S. Makulska, P.M. Korczyk, and P. Garstecki, "Speed of flow of individual droplets in microfluidic channels as a function of the capillary number, volume of droplets and contrast of viscosities", *Lab on a Chip* 11 (21), 3603–3608 (2011)
- [14] H.-H. Jeong, B. Lee, S.H. Jin, S.-G. Jeong, and C.-S. Lee, "A highly addressable static droplet array enabling digital control of a single droplet at pico-volume resolution", *Lab on a Chip* 16 (9), 1698–1707 (2016)
- [15] A.W. Martinez, S.T. Phillips, G.M. Whitesides, and E. Carrilho, "Diagnostics for the Developing World: Microfluidic Paper-Based Analytical Devices", *Analytical Chemistry* 82 (1), 3–10 (2010)
- [16] W. Du, L. Li, K.P. Nichols, and R.F. Ismagilov, "SlipChip", *Lab on a Chip* 9 (16), 2286–2292 (2009)
- [17] X. Niu, S. Gulati, J. B. Edel, and A.J. deMello, "Pillar-induced droplet merging in microfluidic circuits", *Lab on a Chip* 8, 1837 (2008)
- [18] M. Zagnoni and J.M. Cooper, "A microdroplet-based shift register", *Lab on a Chip* 10 (22), 3069–3073 (2010)
- [19] X. Niu, F. Gielen, J.B. Edel, and A.J. deMello, "A microdroplet dilutor for high-throughput screening", *Nature Chemistry* 3 (6), 437–442 (2011)
- [20] C. Chung, M. Lee, K. Char, K.H. Ahn, and S.J. Lee, "Droplet dynamics passing through obstructions in confined microchannel flow", *Microfluidics and Nanofluidics* 9 (6), 1151–1163 (2010), wOS:000284335800013
- [21] M. Sun, S.S. Bithi, and S.A. Vanapalli, "Microfluidic static droplet arrays with tuneable gradients in material composition", *Lab on a Chip* 11 (23), 3949 (2011)
- [22] M. Prakash and N. Gershenfeld, "Microfluidic Bubble Logic", *Science* 315 (5813), 832–835 (2007)
- [23] B. Mosadegh, T. Bersano-Begey, J.Y. Park, M.A. Burns, and S. Takayama, "Next-generation integrated microfluidic circuits", *Lab on a Chip* 11 (17), 2813 (2011)
- [24] P.M. Korczyk, L. Derzsi, S. Jakiela, and P. Garstecki, "Microfluidic traps for hard-wired operations on droplets", *Lab on a Chip* 13 (20), 4096–4102 (2013)
- [25] V. van Steijn, P.M. Korczyk, L. Derzsi, A.R. Abate, D.A. Weitz, and P. Garstecki, "Block-and-break generation of microdroplets with fixed volume", *Biomicrofluidics* 7 (2), 024108–024108–8 (2013)
- [26] D. Zaremba, S. Blonski, and P. Korczyk, "Experimental analysis of modular microfluidic geometries for passive manipulations on droplets", *Book of abstracts, 5th Conference on Nanoand Micromechanics, Wroclaw 2017* 180–182 (2017)
- [27] K.A. Brakke, "The Surface Evolver", *Experimental Mathematics* 1 (2), 141–165 (1992)
- [28] S. Jakiela, P.M. Korczyk, S. Makulska, O. Cybulski, and P. Garstecki, "Discontinuous Transition in a Laminar Fluid Flow: A Change of Flow Topology inside a Droplet Moving in a Micron-Size Channel", *Physical Review Letters* 108 (13), 134501 (2012)
- [29] M. Raffel, C.E. Willert, and J. Kompenhans, *Particle image velocimetry: a practical guide*, Springer (1998)
- [30] S. Blonski, P. Korczyk, and T. Kowalewski, "Analysis of turbulence in a micro-channel emulsifier", *International Journal of Thermal Sciences* 46, 1126–1141 (2007)
- [31] I. Kataoka, "Local instant formulation of two-phase flow", *International Journal of Multiphase Flow* 12 (5), 745–758 (1986)
- [32] K.W. Oh, K. Lee, B. Ahn, and E.P. Furlani, "Design of pressure-driven microfluidic networks using electric circuit analogy", *Lab on a Chip* 12 (3), 515–545 (2012)
- [33] N.A. Mortensen, F. Okkels, and H. Bruus, "Reexamination of Hagen-Poiseuille flow: Shape dependence of the hydraulic resistance in microchannels", *Physical Review E* 71 (5), 057301 (2005)
- [34] K.C. Bhargava, B. Thompson, D. Iqbal, and N. Malmstadt, "Predicting the behavior of microfluidic circuits made from discrete elements", *Scientific Reports* 5 (2015)
- [35] D. Kim, N.C. Chesler, and D.J. Beebe, "A method for dynamic system characterization using hydraulic series resistance", *Lab on a Chip* 6 (5), 639–644 (2006)
- [36] S. Choi, M.G. Lee, and J.-K. Park, "Microfluidic parallel circuit for measurement of hydraulic resistance", *Biomicrofluidics* 4 (3), 034110 (2010)